



Cite this: *Phys. Chem. Chem. Phys.*,  
2018, 20, 23106

Received 12th May 2018,  
Accepted 20th August 2018

DOI: 10.1039/c8cp03028f

rsc.li/pccp

## Non-phase-separated 2D B–C–N alloys via molecule-like carbon doping in 2D BN: atomic structures and optoelectronic properties†

Xiang-Yang Ren,<sup>a</sup> Sha Xia,<sup>a</sup> Xian-Bin Li,<sup>ID\*</sup><sup>ab</sup> Nian-Ke Chen,<sup>a</sup> Xue-Peng Wang,<sup>a</sup> Dan Wang,<sup>a</sup> Zhan-Guo Chen,<sup>a</sup> Shengbai Zhang<sup>ab</sup> and Hong-Bo Sun<sup>ID\*</sup><sup>ac</sup>

Two-dimensional (2D) B–C–N alloys have recently attracted much attention but unfortunately, Chemical Vapor Deposition (CVD) B–C–N alloys typically phase separate. In spite of that, our analysis of the B–C–N alloy fabricated by electron-beam irradiation suggests that non-phase-separated B–C–N may in fact exist with a carbon concentration up to 14 at%. While this analysis points to a new way to overcome the phase-separation in 2D B–C–N, by first-principles calculations, we show that these B–C–N alloys are made of motifs with even numbers of carbon atoms, in particular, dimers or six-fold rings (in a molecule-like form), embedded in a 2D BN network. Moreover, by tuning the carbon concentration, the band gap of the B–C–N alloys can be reduced by 35% from that of BN. Due to a strong overlap of the wavefunctions at the conduction band and valance band edges, the non-phase-separated B–C–N alloys maintain the strong optical absorption of BN.

### Introduction

In recent years, with the development of electronic technology, the integrated density of electronic components is becoming much higher while the sizes of electronic devices are gradually decreasing. For example, the channel length of a field-effect transistor (FET) is approaching its limit and was proved to be as small as 5 nm for a silicon FET in 2017.<sup>1</sup> As a potential candidate to solve the problem, 2D semiconductors with one or several atom thicknesses, exhibit a unique advantage in nanodevices.<sup>2–5</sup> Until now, a variety of 2D semiconductor materials have emerged in electronic devices, such as graphene,<sup>6–8</sup> boron nitride,<sup>9–11</sup> transition-metal disulfide,<sup>10,12,13</sup> black phosphorus,<sup>14,15</sup> and so on.

As the first 2D material, graphene has attracted huge attention since its discovery in 2004<sup>6</sup> due to the high carrier mobility, conductivity, high transparency, and other interesting properties.<sup>6,16–18</sup> As such, it may hold applications in electrodes, transistors, flexible displays, and others.<sup>16,19</sup> However, due to the shortcoming of zero band gap, it is limited to develop logic

or light-emission applications. Similarly, 2D hexagonal boron nitride (h-BN) also has a honeycomb structure like graphene, it is a strong antioxidant which can be stable in the air up to 900 °C<sup>20</sup> and it has a 6.06 eV<sup>21</sup> or 6.07 eV<sup>22</sup> optical band gap. To take advantages of graphene and 2D BN, it has been proposed to combine them to be a new kind of 2D alloyed semiconductor for electronics or optoelectronics.<sup>23–26</sup>

Up to now, both experimental and theoretical studies have made a lot of effort to achieve 2D B–C–N alloys. For theoretical studies, in 2011 Berseneva *et al.* showed that in 2D BN the replacement of B/N with carbon is affected not only by irradiation but also by the energetics of the carbon atomic configurations.<sup>27</sup> In 2013, based on first-principles calculations, Pan *et al.* found that the reaction-potential barrier of B replacing C in graphene can be reduced on a metallic ruthenium substrate.<sup>28</sup> Accordingly, they successfully achieved B-doped graphene in experiment. In 2015, with the particle-swarm-optimization technique as well as the cluster-expansion method, Zhang *et al.* confirmed that the structures of 2D B–C–N systems tend to phase separate.<sup>29</sup> Their calculations showed that the band gaps of B–C–N systems were adjustable from that of graphene to that of BN. They also found most of the proposed candidates had direct band gaps and possessed good light absorption in the visible range. For experimental studies, in 2010, Ci *et al.* successfully synthesized B–C–N systems by using methane (CH<sub>4</sub>) and ammonia borane (NH<sub>3</sub>–BH<sub>3</sub>) as precursors *via* a thermal catalytic method. However, after characterization, these composites were phase separated.<sup>30</sup> Nevertheless, in 2015, Wang *et al.*, on the

<sup>a</sup> State Key Laboratory of Integrated Optoelectronics, College of Electronic Science and Engineering, Jilin University, Changchun 130012, China.

E-mail: lixianbin@jlu.edu.cn

<sup>b</sup> Department of Physics, Applied Physics, and Astronomy, Rensselaer Polytechnic Institute, Troy, New York 12180, USA

<sup>c</sup> State Key Lab of Precision Measurement Technology and Instruments,

Department of Precision Instrument, Tsinghua University, Beijing, 100084, China

† Electronic supplementary information (ESI) available. See DOI: 10.1039/c8cp03028f

basis of Ci *et al.*<sup>30</sup> changed the synthetic precursors to trimethyl borane [B(CH<sub>3</sub>)<sub>3</sub>] and ammonia gas (NH<sub>3</sub>). They claimed that B–C–N systems were successfully synthesized in some sense.<sup>31</sup> The main difference between the two experimental studies is that the former precursors contain a large number of B–N bonds, while the latter contain a large number of B–C bonds.

Although research of B–C–N systems is still going on, the problem of phase separation is still not solved. In this work, in order to obtain the alloyed structure of 2D B–C–N without phase separation, based on first-principles calculations and analyses of previous experiments, we dope carbon atoms into 2D BN. We find that even-number carbon defect molecule-like motifs, such as the dimer and six-fold ring, manifest a lower formation energy. We construct non-phase-separated alloys of B–C–N *via* doping the molecule-like carbon motifs in 2D BN with concentrations from 0% to 14% (such concentrations can be found in experiment). We find that the band gaps can be modified as low as 65% of that of BN, indicating a tuneable band gap. We also calculate the real-space charge density distribution for the conduction band minimum (CBM) and valence band maximum (VBM). It is found that the CBM and VBM are both from carbon motifs as molecule-like states. The imaginary part of the dielectric constant displays a good photonic absorption. The study offers an idea to overcome the difficulty of phase separation for synthesizing 2D B–C–N.

## Simulation methods

In this work, density functional theory (DFT)<sup>32,33</sup> is employed as implemented in the Vienna *Ab initio* Simulation Package (VASP) codes.<sup>34</sup> The projector augmented wave basis<sup>35</sup> and Perdew–Burke–Ernzerhof (PBE) functional<sup>36</sup> (a kind of generalized gradient approximation (GGA)<sup>37</sup>) are adopted. An 8 × 8 × 1 honeycomb supercell with 128 atoms is used throughout for calculations of 2D materials. All the atoms are relaxed until the Hellman–Feynman forces on individual atoms are less than 0.01 eV Å<sup>-1</sup>. The cut-off energy of the plane-wave basis is 520 eV. The 1 × 1 × 1 Monkhorst–Pack *k*-point mesh grid is used for atomic relaxation. Spin polarization has also been considered. For comparing formation energies of other alloys, a 192-atom model of Mo<sub>0.86</sub>W<sub>0.14</sub>S<sub>2</sub> alloy is evaluated with a cutoff energy of 360 eV and *k*-point mesh grid of 1 × 1 × 1.

To determine the possibility of the existence of various C defects in 2D BN, their formation energies are calculated. Usually, the formation energy  $E_f(X_Y)$  of element X replacing element Y in a host material<sup>38–41</sup> is given as,

$$E_f(X_Y) = E_{\text{tot}}(X_Y) - E_{\text{tot}}(\text{bulk}) - \mu_X(\text{solid/gas}) - \mu_X' + \mu_Y(\text{solid/gas}) + \mu_Y' \quad (1)$$

where X is the impurity atom and Y is the host atom replaced by X.  $E_{\text{tot}}(X_Y)$  is the total energy of the defective supercell (X replacing Y), and  $E_{\text{tot}}(\text{bulk})$  is the total energy of the perfect supercell without a defect.  $\mu_X'$  and  $\mu_Y'$  are the chemical potentials of elements X and Y referenced to their energies in stable elementary forms (solid or gas), *i.e.*  $\mu_X(\text{solid/gas})$  and  $\mu_Y(\text{solid/gas})$ . Here,  $\mu_{N(N_2\text{gas})}$ ,

$\mu_{B(\text{solid})}$ ,  $\mu_{C(\text{graphene})}$  are used. All the defects are analysed in their neutral states. Since the formation of a defect is determined by experimental growth conditions (such as B-rich conditions, N-rich conditions, or between them), the formation energy of a defect depends on different chemical potentials. Under thermal equilibrium, the chemical potentials of host atoms must satisfy  $\mu_N' + \mu_B' = \Delta H_f(\text{BN})$ , where  $\Delta H_f(\text{BN})$  is the formation enthalpy of the 2D BN. Under different experimental conditions,  $\mu_B'$  and  $\mu_N'$  vary in the ranges as below,

$$\begin{aligned} & (\text{B-poor conditions}) \Delta H_f(\text{BN}) \leq \mu_B' \leq 0 \quad (\text{B-rich conditions}) \\ & \quad (2) \end{aligned}$$

$$\begin{aligned} & (\text{N-poor conditions}) \Delta H_f(\text{BN}) \leq \mu_N' \leq 0 \quad (\text{N-rich conditions}) \\ & \quad (3) \end{aligned}$$

To calculate the dielectric function, we first perform the geometry optimization of the constructed models and then get their ground-state electronic structure by a higher-precision static calculation. Then, we get the wavefunction from the “WAVECAR” document as an input. The parameter “LOPTICS = .TRUE.” is set up to calculate the frequency dependent dielectric matrix in VASP based on the calculated single-particle electronic structure. The imaginary part is determined by a summation over the states using the equation:

$$\begin{aligned} \varepsilon_{\alpha\beta}^{(2)}(\omega) = & \frac{4\pi^2e^2}{\Omega} \lim_{q \rightarrow 0} \frac{1}{q^2} \sum_{c,v,K} 2w_K \delta(\varepsilon_{cK} - \varepsilon_{vK} - \omega) \\ & \times \langle u_{cK} + e_{\alpha q} | u_{vK} \rangle \langle u_{cK} + e_{\beta q} | u_{vK} \rangle^* \end{aligned} \quad (4)$$

where the indices c and v refer to conduction and valence band states, respectively.  $u_{cK}$  and  $u_{vK}$  are the cell periodic part of the orbitals at K for conduction band states and valence band states, respectively. Notice: the calculation of the dielectric function requires a large enough number of empty conduction bands (here, we set 776 empty bands in our 128-atom models).

## Results and discussion

In order to solve the problem of phase separation and find possible alloy structures for 2D B–C–N, we study the local C defects in 2D BN. We focus on carbon motifs with the number of atoms from 1 to 6. The structures of 35 possible candidates are shown in Fig. 1(a). For these defects, their formation energies are calculated in the condition of  $\mu'_B = \mu'_N$ , see Fig. 1(b). The formation energies in B rich or N rich conditions are also evaluated in Fig. S1 and S2 (ESI†). Here, the notation “*m-n*” for the models in Fig. 1 is explained as follows: *m* represents the number of carbons for a defect and *n* represents the *n*th defect. From the trend of energies in Fig. 1(b), the carbon defects with an even atom number generally have lower formation energies than those with an odd atom number. Especially, we highlight three typical even-number defects in the inset of Fig. 1(b). Therefore, the carbon defects with an even number should exist more easily in BN.

In order to further illustrate the rule on defect formation, we take 6-carbon defects as examples. Fig. S3 (ESI†) displays

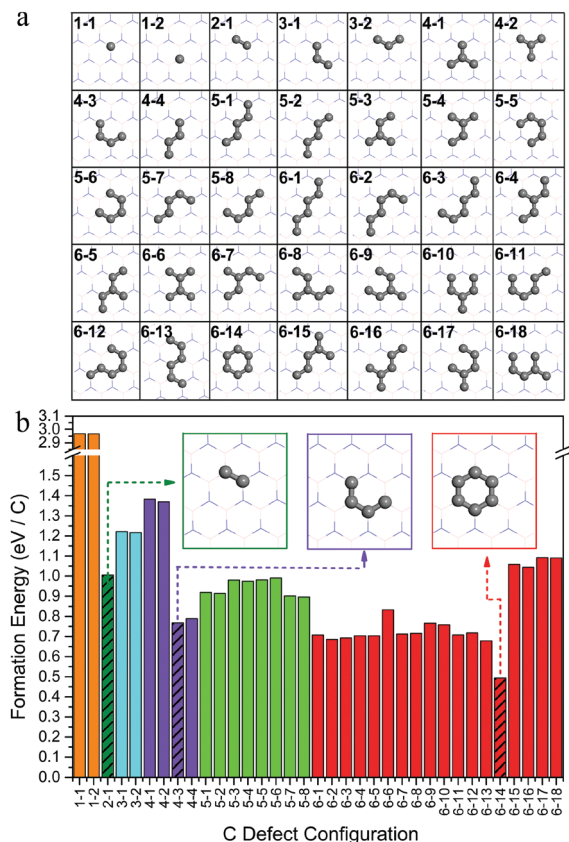


**Fig. 1** (a) Possible carbon motifs doped in 2D BN. (b) Formation energy (per atom) of C defects in 2D BN in the condition of  $\mu'_B = \mu'_N$ . Different colours represent the motifs with different carbon numbers. The motifs with relatively low energy are highlighted in the insets. Color coding of atoms: pink for B, blue for N, and grey for C. The notation “ $m-n$ ” is explained in the main text.

their motifs. For the 6-17 and 6-18 motifs (where  $2N + 4B$  and  $2B + 4N$  are replaced by 6 carbons, respectively), there are two fewer electrons when replacing  $2N + 4B$  and two more electrons when replacing  $2B + 4N$ . As such, their formation energies are significantly larger due to breaking electron-number balance. In contrast, the  $3N + 3B$  replacements (*i.e.* equal number replacement for N and B) should be more reasonable. That is because the total number of valence electrons of 6 carbons is just equal to that of the replaced atoms. In fact, the 6-14, 6-2, 6-10, and 6-6 defects indeed show the case. Among them, the 6-carbon honeycomb ring or say six-fold ring (6-14) holds the lowest formation energy. This is easy to be understood by the fact that the strong carbon–carbon covalent bond further stabilizes the defect. Therefore, the carbon dimer (2-1), four connected carbons inside a honeycomb ring (4-3), and the six-fold ring (6-14) are the most feasible defects existing in 2D BN.

In fact, an ideal 2D alloy should be the one belonging to complete solid solution systems, such as 2D  $Mo_{1-x}W_xS_2$ ,  $0 < x < 1$ .<sup>42–44</sup> Here, we take a 14% concentration of dopant of  $Mo_{1-x}W_xS_2$  as a reference, *i.e.*  $Mo_{0.86}W_{0.14}S_2$ , see Fig. 2(a). Fig. 2(d) indeed shows the formation energy for every W doped into  $MoS_2$  can be as small as 0.14 eV. However, the case of a

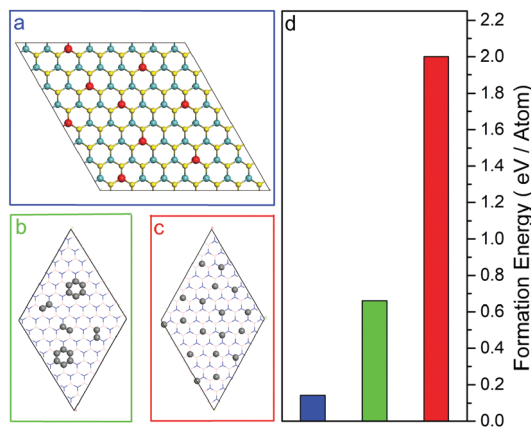


**Fig. 2** Strategy to synthesize B–C–N semiconductors with lower energy. (a) W alloying  $MoS_2$  with individual atom doping. (b) C alloying 2D BN with molecule-like doping (*i.e.* the C dimer or 6-fold ring). (c) C alloying 2D BN with individual atom doping. (d) Average formation energy per dopant for the three cases above. The case for (a) is  $Mo_{0.86}W_{0.14}S_2$  and the cases for (b) and (c) are  $B_{0.43}N_{0.43}C_{0.14}$ . In (a) the light blue, red, and yellow balls are for the Mo, W, and S atoms, respectively. The color coding for B–C–N is the same as Fig. 1.

complete solid solution for  $(BN)_{(1-x)/2}C_x$  is very difficult since the formation energy of every individual C doped into the BN lattice [see Fig. 2(c)] is as high as 2.00 eV. That explains why many previous results support a conclusion of phase separation for 2D B–C–N systems no matter from theory<sup>29,45,46</sup> or experiment.<sup>30,31,47–49</sup> However, as early as 2010, Krivanek *et al.* carried out an interesting experiment to bombard a single BN layer by an electron beam. As a result, some amount of atomic holes were opened up to facilitate the doping of C atoms as well as other elements. In their Scanning Transmission Electron Microscope (STEM) analyses, annular dark-field imaging in an aberration-corrected STEM operated at a 60 kV primary voltage can identify the positions of every atom. They showed that C atoms could be in the forms of the dimer (*i.e.* the 2-1 model) and six-fold ring (*i.e.* the 6-14 model) embedded into 2D BN instead of individual atom doping.<sup>50</sup> In fact, some methods, for example, analyzing the electrostatic potential for atomic models, are also useful to identify the atomic picture from the TEM image.<sup>51</sup> These observations well coincide with the present discovery of relatively low formation energy of even-number carbon defects. As such, molecule-like carbon doping in 2D BN should be a feasible route to construct a 2D B–C–N alloy. Fig. 2(b) shows one such case with 14% carbon doping. Although its formation energy (0.66 eV) is still higher than that of  $Mo_{0.86}W_{0.14}S_2$ , it is much lower than that of individual C doping. In fact, some special manufacturing technique could overcome the energy of molecule-like doping, such as the electron-beam-bombardment facilitated doping technique, which is mentioned above.<sup>50</sup> In their TEM observation, as high as 14% of carbon atoms can be doped into the 2D BN plane in the form of the dimer or six-fold ring; see the inset of the TEM picture in Fig. 3(a). Therefore, the present calculation and the experimental analysis offer a possible route to synthesize 2D B–C–N alloys without phase separation.

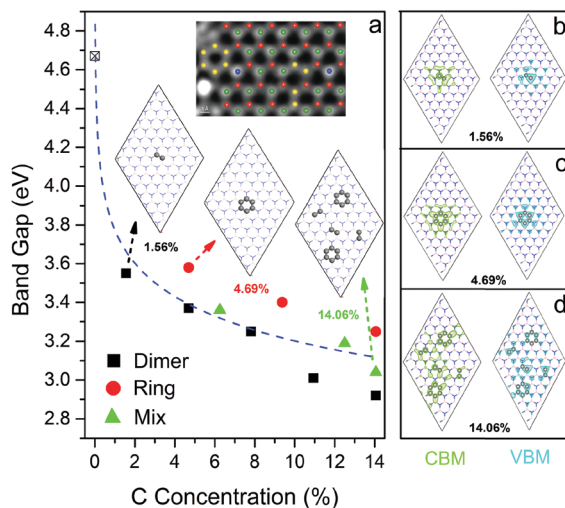


**Fig. 3** Electronic properties of the proposed 2D B–C–N alloys. (a) GGA band gap vs. carbon concentration. Here, black squares represent the dimer models; red circles stand for the six-fold-ring models; and green triangles represent their mixing models. Distribution of CBM and VBM states in real space for the models with concentrations of (b) 1.56%, (c) 4.69%, and (d) 14.06%. A TEM experimental picture is reproduced with permission from ref. 50 (Copyright 2010, Nature Publishing Group) in the inset for illustration of our proposed B–C–N models without phase separation. In the TEM picture, atoms are identified as red for B, green for N, yellow for C, and blue for O.

Next, we employ these two molecule-like motifs (*i.e.* the carbon dimer and six-fold ring) to construct non-phase-separated B–C–N with experimentally feasible concentrations. Fig. 3(a) shows the band gaps of these B–C–N alloys decrease gradually with increasing carbon concentration. According to GGA calculations, we demonstrate the gaps can be modified from 100% to 65% of the gap of 2D BN when the dopant concentrations vary from 0% to 14%. That means a tunable electronic property for these models. In Fig. 4 and Fig. S4 of ESI,† the band structures [Fig. 4(a) and (c)] and the PDOS (partial density of states) [Fig. 4(b) and (d)] of the typical B–C–N models are

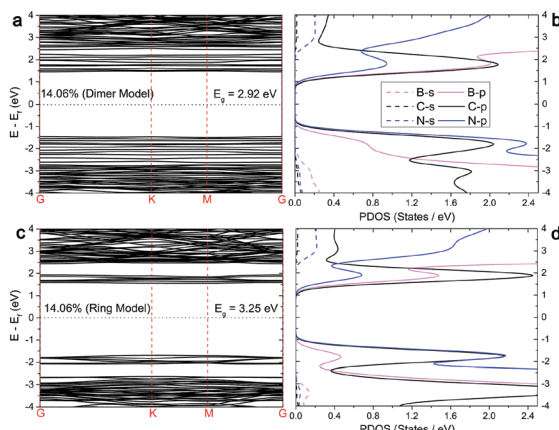


**Fig. 4** Band structures and partial DOS (PDOS) of B–C–N alloy models with a carbon concentration of 14.06%. (a) and (c) are the band structures for the dimer model and ring model, respectively. (b) and (d) are the PDOS of (a) and (c), respectively.

further shown. From the PDOS, we can observe that the carbon atoms mainly contribute to the VBM and CBM. But the bonding situations are slightly different between the CBMs and VBMs. Their CBMs are mainly composed of carbon p orbitals and boron p orbitals while the VBMs are mainly composed of carbon p orbitals and nitrogen p orbitals. We also fit the curve of band gap vs. carbon concentration to see the trend. Three representative models with concentrations of 1.56%, 4.69%, and 14.06% are highlighted in the inset of Fig. 3(a). Their corresponding VBM and CBM states are also plotted in real space in Fig. 3(b)–(d). It is interestingly noted that the distribution of CBMs and VBMs for these B–C–N models are all around the carbon molecule-like motifs, no matter based on dimers, or six-fold rings, or their mixtures. In other words, such kinds of B–C–N alloys hold molecule-like electronic states in their band edge which indicate their carriers should be in the form of hopping or tunneling for transportation.

Usually, molecule-like states in semiconductors could benefit light absorption or light emission.<sup>52</sup> In order to explore the application in optoelectronics, we calculate their absorption spectrum, *i.e.* the imaginary part of dielectric function  $\epsilon_2$  for these non-phase-separated B–C–N models. Fig. 5 shows the in-plane  $\epsilon_2$  (x-axis direction, the case for the y-axis direction is almost the same). First of all, the molecule-like CBM and VBM together produce a strong absorption within the normal 2D BN gap, which is reflected by their strong overlap of wavefunctions to facilitate electron transition. With increasing carbon concentration, the start-up of the absorption is redshifted and the intensity become stronger. This means such kinds of 2D B–C–N alloy are especially suitable for optoelectronics, such as high sensitive detectors, light emitting diodes (LEDs), and light amplification by stimulated emission of radiation (LASER) with designed wavelengths.

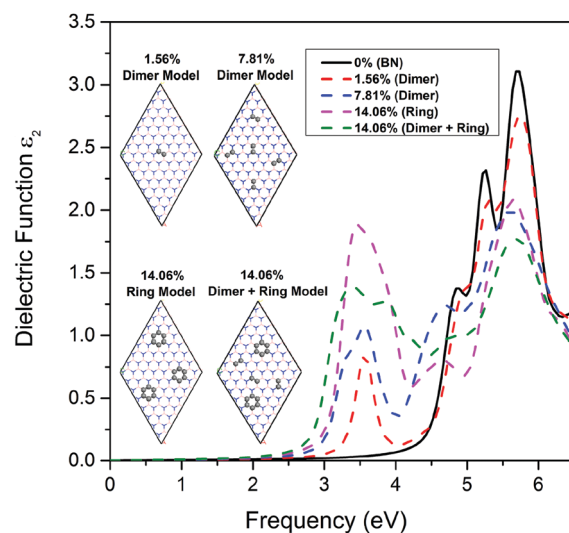


**Fig. 5** In-plane dielectric function  $\epsilon_2$  of the proposed B–C–N models. The solid line is for the pure 2D BN and the dashed lines are for the proposed B–C–N models at their carbon concentrations up to an experimentally feasible 14%.

## Conclusions

In sum, we find that the most likely carbon defects doped into 2D BN are the even-number molecule-like motifs, such as the dimer or six-fold ring. Thus, using these motifs, we construct and propose 2D B-C-N models without phase separation. While their formation energy is still not low enough to form at mild thermal equilibrium conditions, the proposed 2D B-C-N models could be realized by certain techniques, such as the electron-beam facilitated doping technique.<sup>50</sup> With experimentally feasible carbon concentrations (up to 14%), the proposed models have tuneable band gaps from 100% to 65% of that of 2D BN. Their CBMs and VBM all locate around carbon motifs. The strong overlap of the wavefunction of these frontier orbitals makes the systems especially suitable for optoelectronics. The present studies offer a feasible route to overcome the main challenge of the phase separation problem for 2D B-C-N alloy fabrication. It will benefit their application in electronics.

The idea of molecule-like doping should be a useful idea to synthesize other 2D alloys which are easily phase separated. In fact, before the theoretical study (two years ago), an experimental team led by Prof. Jianlin Liu at University of California, Riverside invited us to find some possible structures for 2D B-C-N. Therefore, in the next step, we and the experimental colleagues will try to fabricate the proposed 2D B-C-N models. Furthermore, from a theoretical perspective, the methods to get possible n- or p-type conductivity in these B-C-N models should be also worth exploring in the near future.

## Conflicts of interest

There are no conflicts to declare.

## Acknowledgements

The work was supported by National Natural Science Foundation of China (No. 11874171, 61775077, 61474055), and 973 Program (No. 2014CB921303). We acknowledge the High-Performance Computing Center (HPCC) at Jilin University for calculation resources. Work at RPI was supported by the Department of Energy under Grant No. DE-SC0002623. We thank Prof. Jianlin Liu in University of California, Riverside for his helpful discussion.

## References

- N. Loubet, T. Hook, P. Montanini, C. W. Yeung, S. Kanakasabapathy, M. Guillom, T. Yamashita, J. Zhang, X. Miao and J. Wang, presented in part at the 2017 Symposium on VLSI Technology, Kyoto (Japan), 2017.
- L. X. Zhu, F. Y. Liu, H. T. Lin, J. J. Hu, Z. F. Yu, X. R. Wang and S. H. Fan, *Light: Sci. Appl.*, 2016, **5**, e16052.
- X. P. Wang, X. B. Li, N. K. Chen, J. H. Zhao, Q. D. Chen and H. B. Sun, *Phys. Chem. Chem. Phys.*, 2018, **20**, 6945–6950.
- D. Wang, X. B. Li, D. Han, W. Q. Tian and H. B. Sun, *Nano Today*, 2017, **16**, 30–45.
- X. B. Li, S. Y. Xie, H. Zheng, W. Q. Tian and H. B. Sun, *Nanoscale*, 2015, **7**, 18863–18871.
- K. S. Novoselov, A. K. Geim, S. V. Morozov, D. Jiang, Y. Zhang, S. V. Dubonos, I. V. Grigorieva and A. A. Firsov, *Science*, 2004, **306**, 666.
- D. Rodrigo, A. Tittl, O. Limaj, F. J. G. d. Abajo, V. Pruneri and H. Altug, *Light: Sci. Appl.*, 2017, **6**, e16277.
- W. Strek, B. Cichy, L. Radosinski, P. Gluchowski, L. Marciniak, M. Lukaszewicz and D. Hreniak, *Light: Sci. Appl.*, 2015, **4**, e237.
- D. Pacilé, J. C. Meyer, Ç. Ö. Girit and A. Zettl, *Appl. Phys. Lett.*, 2008, **92**, 133107.
- M. Xu, T. Liang, M. Shi and H. Chen, *Chem. Rev.*, 2013, **113**, 3766–3798.
- M. Autore, P. Li, I. Dolado, F. J. Alfaro-Mozaz, R. Esteban, A. Atxabal, F. Casanova, L. E. Hueso, P. Alonso-González, J. Aizpurua, A. Y. Nikitin, S. Vélez and R. Hillenbrand, *Light: Sci. Appl.*, 2018, **7**, 17172.
- Q. H. Wang, K. Kalantazadeh, A. Kis, J. N. Coleman and M. S. Strano, *Nat. Nanotechnol.*, 2012, **7**, 699–712.
- J. Yang, Z. Wang, F. Wang, R. J. Xu, J. Tao, S. Zhang, Q. H. Qin, B. Luther-Davies, C. Jagadish, Z. F. Yu and Y. R. Lu, *Light: Sci. Appl.*, 2016, **5**, e16046.
- F. Xia, H. Wang and Y. Jia, *Nat. Commun.*, 2014, **5**, 4458.
- Y. Abate, S. Gamage, Z. Li, V. Babicheva, M. H. Javani, H. Wang, S. B. Cronin and M. I. Stockman, *Light: Sci. Appl.*, 2016, **5**, e16162.
- W. H. Lee, J. Park, S. H. Sim, S. B. Jo, K. S. Kim, B. H. Hong and K. Cho, *Adv. Mater.*, 2011, **23**, 1752–1756.
- X. Li, Y. Zhu, W. Cai, M. Borysiak, B. Han, D. Chen, R. D. Piner, L. Colombo and R. S. Ruoff, *Nano Lett.*, 2009, **9**, 4359–4363.
- K. S. Kim, Y. Zhao, H. Jang, S. Y. Lee, J. M. Kim, K. S. Kim, J.-H. Ahn, P. Kim, J.-Y. Choi and B. H. Hong, *Nature*, 2009, **457**, 706–710.
- W.-H. Wang, R.-X. Du, X.-T. Guo, J. Jiang, W.-W. Zhao, Z.-H. Ni, X.-R. Wang, Y.-M. You and Z.-H. Ni, *Light: Sci. Appl.*, 2017, **6**, e17113.
- H. Zeng, C. Zhi, Z. Zhang, X. Wei, X. Wang, W. Guo, Y. Bando and D. Golberg, *Nano Lett.*, 2010, **10**, 5049.
- G. Kim, A. R. Jang, H. Y. Jeong, Z. Lee, D. J. Kang and H. S. Shin, *Nano Lett.*, 2013, **13**, 1834–1839.
- L. F. Wang, B. Wu, J. S. Chen, H. T. Liu, P. A. Hu and Y. Q. Liu, *Adv. Mater.*, 2014, **26**, 1559–1564.
- Y. Miyamoto, M. L. Cohen and S. G. Louie, *Phys. Rev. B: Condens. Matter Mater. Phys.*, 1995, **52**, 14971–14975.
- S. Azevedo, *Eur. Phys. J. B*, 2005, **44**, 203–207.
- O. Stephan, P. M. Ajayan, C. Colliex, P. Redlich, J. M. Lambert, P. Bernier and P. Lefin, *Science*, 1994, **266**, 1683–1685.
- H. Pan, Y. P. Feng and J. Lin, *Phys. Rev. B: Condens. Matter Mater. Phys.*, 2006, **74**, 045409.
- N. Berseneva, A. V. Krasheninnikov and R. M. Nieminen, *Phys. Rev. Lett.*, 2011, **107**, 035501.
- L. Pan, Y. Que, H. Chen, D. Wang, J. Li, C. Shen, W. Xiao, S. Du, H. Gao and S. T. Pantelides, *Nano Lett.*, 2015, **15**, 6464–6468.

- 29 M. Zhang, G. Gao, A. Kutana, Y. Wang, X. Zou, J. S. Tse, B. I. Yakobson, H. Li, H. Liu and Y. Ma, *Nanoscale*, 2015, **7**, 12023.
- 30 L. Ci, L. Song, C. Jin, D. Jariwala, D. Wu, Y. Li, A. Srivastava, Z. F. Wang, K. Storr and L. Balicas, *Nat. Mater.*, 2010, **9**, 430–435.
- 31 H. Wang, C. Zhao, L. Liu, Z. Xu, J. Wei, W. Wang, X. Bai and E. Wang, *Nano Res.*, 2016, **9**, 1221–1235.
- 32 P. Hohenberg and W. Kohn, *Phys. Rev.*, 1964, **136**, B864–B871.
- 33 W. Kohn and L. J. Sham, *Phys. Rev.*, 1965, **140**, A1133–A1138.
- 34 G. Kresse and J. Furthmüller, *Phys. Rev. B: Condens. Matter Mater. Phys.*, 1996, **54**, 11169–11186.
- 35 P. E. Blöchl, *Phys. Rev. B: Condens. Matter Mater. Phys.*, 1994, **50**, 17953–17979.
- 36 J. P. Perdew, K. Burke and M. Ernzerhof, *Phys. Rev. Lett.*, 1996, **77**, 3865–3868.
- 37 J. P. Perdew and W. Yue, *Phys. Rev. B: Condens. Matter Mater. Phys.*, 1986, **33**, 8800–8802.
- 38 S. B. Zhang and J. E. Northrup, *Phys. Rev. Lett.*, 1991, **67**, 2339.
- 39 D. Han, D. West, X. B. Li, S. Y. Xie, H. B. Sun and S. B. Zhang, *Phys. Rev. B: Condens. Matter Mater. Phys.*, 2010, **82**, 155132.
- 40 D. Wang, D. Han, X. B. Li, N. K. Chen, D. West, V. Meunier, S. B. Zhang and H. B. Sun, *Phys. Rev. B: Condens. Matter Mater. Phys.*, 2017, **96**, 155424.
- 41 D. Wang, D. Han, X. B. Li, S. Y. Xie, N. K. Chen, W. Q. Tian, D. West, H. B. Sun and S. B. Zhang, *Phys. Rev. Lett.*, 2015, **114**, 196801.
- 42 J. Y. Xi, T. Q. Zhao, D. Wang and Z. G. Shuai, *J. Phys. Chem. Lett.*, 2014, **5**, 285–291.
- 43 D. O. Dumcenco, H. Kobayashi, Z. Liu, Y. S. Huang and K. Suenaga, *Nat. Commun.*, 2013, **4**, 1351.
- 44 H. F. Liu, K. K. A. Antwi, S. Chua and D. Z. Chi, *Nanoscale*, 2014, **6**, 624–629.
- 45 I. Guilhon, M. Marques, L. K. Teles and F. Bechstedt, *Phys. Rev. B: Condens. Matter Mater. Phys.*, 2017, **95**, 035407.
- 46 K. Yuge, *Phys. Rev. B: Condens. Matter Mater. Phys.*, 2009, **79**, 144109.
- 47 M. O. Watanabe, S. Itoh, K. Mizushima and T. Sasaki, *Appl. Phys. Lett.*, 1996, **68**, 2962–2964.
- 48 M. R. Uddin, S. Majety, J. Li, J. Y. Lin and H. X. Jiang, *J. Appl. Phys.*, 2014, **115**, 093509.
- 49 Y. Gong, G. Shi, Z. Zhang, W. Zhou, J. Jung, W. Gao, L. Ma, Y. Yang, S. Yang and Y. Ge, *Nat. Commun.*, 2014, **5**, 3193.
- 50 O. L. Krivanek, M. F. Chisholm, V. Nicolosi, T. J. Pennycook, G. J. Corbin, N. Dellby, M. F. Murfitt, C. S. Own, Z. S. Szilagyi, M. P. Oxley, S. T. Pantelides and S. J. Pennycook, *Nature*, 2010, **464**, 571–574.
- 51 S. Kurasch, J. C. Meyer, D. Kunzel, A. Gross and U. Kaiser, *Beilstein J. Nanotechnol.*, 2011, **2**, 394–404.
- 52 S. B. Zhang, S. H. Wei and A. Zunger, *Phys. Rev. B: Condens. Matter Mater. Phys.*, 2001, **63**, 075205.